

Document downloaded from:

<http://hdl.handle.net/10251/149934>

This paper must be cited as:

Mateo-Mateo, D.; Albero-Sancho, J.; García Gómez, H. (2017). Photoassisted methanation using Cu₂O nanoparticles supported on graphene as a photocatalyst. *Energy & Environmental Science*. 10(11):2392-2400. <https://doi.org/10.1039/c7ee02287e>



The final publication is available at

<https://doi.org/10.1039/c7ee02287e>

Copyright The Royal Society of Chemistry

Additional Information

Photoassisted methanation using Cu₂O nanoparticles supported on graphene as photocatalyst.

Diego Mateo,^a Josep Albero^a and Hermenegildo García*^a

Received 00th January 20xx,
Accepted 00th January 20xx

DOI: 10.1039/x0xx00000x

www.rsc.org/

Photoassisted CO₂ methanation can be carried out efficiently at 250 °C using Cu₂O nanoparticles supported on few layer graphene (Cu₂O/G) as photocatalyst. The Cu₂O/G photocatalyst has been prepared by chemical reduction of a Cu salt (Cu(NO₃)₂) with ethylene glycol in the presence of defective graphene obtained from the pyrolysis of alginate acid at 900 °C under Ar flow. Using this photocatalyst a maximum specific CH₄ formation rate of 14.93 mmol/g_{Cu₂O}·h and apparent quantum yield of 7.84 % was achieved, which is one of the highest reported values for the gas-phase methanation reaction at temperatures below Sabatier reaction (> 350 °C). It was found that the most probable reaction mechanism involves photoinduced electron transfer from the Cu₂O/G photocatalyst to CO₂, while evidence indicates that light-induced local temperature increase and H₂ activation are negligible. The role of the temperature in the process has been studied, the available data suggesting that heating is needed to desorb the H₂O formed as product during the methanation. The most probable reaction mechanism seems to follow dissociative pathway involving detachment of oxygen atoms from CO₂.

Introduction

The quest for renewable fuels for transportation and the growing concern on greenhouse gas emissions has led to consider the use of CO₂ as feedstock for fuel preparation.¹⁻³ In this regard, one of the most promising approaches to convert CO₂ is light-assisted reduction using natural solar light as source.^{4, 5} Since the seminal paper of Fujishima and Honda,⁶ numerous semiconducting materials, such as, metal oxides, metal sulfides and layered double hydroxides (LHD) among others, have been explored as photocatalysts for the light-promoted reduction of CO₂.⁷ Although, TiO₂-based photocatalysts have been the most widely studied due to their low cost and high stability, their wide-bandgap and high electron-hole recombination rate have motivated the interest in exploring alternative materials and developing strategies to overcome these drawbacks, including sensitization with dyes or metallic complexes⁸ and their modification with metal co-catalysts.^{9, 10}

Graphene (G) is a one atom thick 2D material of sp²-hybridized carbon atoms in hexagonal arrangement. This material has attracted much interest in recent years due to its unique physical and chemical properties such high specific surface area, outstanding charge mobility, photochemical stability, etc. These properties have been found very convenient in the use of

G-based materials as additive in photocatalytic systems¹¹ or as metal free photocatalysts¹². In this context, the use of G as co-catalyst to enhance the efficiency of TiO₂, WO₃ and other semiconducting metal oxides has been amply reported in the photocatalytic CO₂ reduction¹¹. Considering that G is a zero bandgap semiconductor, its role in these photocatalytic systems, besides as support of the photoresponsive components^{13, 14}, is to favour charge separation and to act as co-catalyst^{15, 16}. Indeed, it has been proved that the lifetime of the photogenerated charges in the semiconductors increases when they are in contact with G.¹⁷

Since current efficiencies and conversion rates of artificial photosynthesis, meaning the endothermic reaction of CO₂ with H₂O promoted by a photocatalytic system, is far from any industrial process, one of the alternative photocatalytic processes that is attracting much current interest is light-assisted CO₂ methanation to form CH₄. H₂ required in the methanation would be generated from H₂O by electrolysis using renewable electricity and it can become available in large quantities because it will be a way to store electricity into chemicals when there is a surplus of production vs. consumption. Water electrolysis at high current densities can be carried out with efficiencies over 50%, but, then, the problem would be H₂ storage and its use as transportation fuel that most probably would require further transformation into a different compound. H₂ reaction with CO₂ could be, then, one of the preferred reactions considering also the availability of CO₂ from conventional power plants and the convenience to avoid its emission to the atmosphere.

Methanation of CO₂, known as the Sabatier reaction, is an exothermic reaction (eq. 1) that can be carried out catalytically

^a Instituto Universitario de Tecnología Química CSIC-UPV, Universitat Politècnica de Valencia, Av. De los Narajos s/n, 46022 Valencia. E-mail: hgarcia@qim.upv.es
Electronic Supplementary Information (ESI) available: [details of any supplementary information available should be included here]. See DOI: 10.1039/x0xx00000x

at high rates at temperatures above to 300 °C, typically 450 °C. However, it would be advantageous to develop efficient photo-assisted methanation using natural sunlight for the process, since solar light can provide the energy required in the large scale implementation of this reaction.



Although the use of carbon based materials as G¹⁸ and graphene oxide (GO),¹⁹ among others (graphite, carbon nanotubes or graphene quantum dots)^{20, 21} has been widely studied as support of metal or metal oxide nanoparticles (NPs) in the photo- and electrocatalytic CH₃OH and CH₄ production in aqueous media, the gas phase photocatalytic CO₂ methanation has been much less explored. Only recently, Chai et al. have reported the preparation of a hybrid 2D material composed by reduced graphene oxide (rGO) and protonated g-C₃N₄ for the photocatalytic CO₂ methanation in gas phase, which rendered 13.93 μmol/g_{cat}.²²

In this manuscript we describe the photo-assisted gas-phase methanation by reacting stoichiometric amounts of CO₂ and H₂ in the presence of Cu₂O NPs supported on G (Cu₂O/G) at temperatures lower than required in the Sabatier reaction (≤ 250 °C). This renders an optimum 14.93 mmol/g_{Cu}·h of CH₄ at 250 °C upon Xe lamp irradiation at 200 mW/cm². The origin of this high production rate comes from the synergetic effect between G and the Cu₂O NPs, where G, obtained from the pyrolysis of alginic acid, supports homogeneously distributed Cu₂O NPs and enhances charge separation by migration of conduction band electrons generated in Cu₂O to G.

Experimental

Materials and procedures

Few-layers G (100 mg) dispersed in ethylene glycol (40 mL) was obtained from the pyrolysis under Ar flow at 900 °C of alginic acid sodium salt from brown algae (Aldrich) and subsequent sonication in ethylene glycol at 700 W for 1 h, as reported before²³. Cu(NO₃)₂ was added to the suspension and Cu²⁺ reduction was then performed at 120 °C for 24 h under continuous stirring. The Cu₂O/G sample was finally separated from ethylene glycol by filtration and washed exhaustively with water and with acetone. The resulting material was dried in a vacuum desiccator at 110 °C to remove the remaining water.

The amount of copper present in the samples was determined by inductively coupled plasma-optical emission spectrometry (ICP-OES) by dissolving the Cu present in Cu₂O/G with *aqua regia* at room temperature for 3 h and analyzing the Cu content of the resulting solution.

Ethanol suspension of Cu₂O (< 350 nm) was purchased from Aldrich (1.5% (w/v)).

Characterization

Powder XRD patterns were recorded on a Shimadzu XRD-7000 diffractometer using Cu Kα radiation (λ = 1.5418 Å, 40 kV, 40 mA) at a scanning speed of 1 ° per min in the 10-80 ° 2θ range. Raman spectra were collected with a Horiba Jobin Yvon-Labram HR UV-Visible-NIR (200-1,600 nm) Raman Microscope Spectrometer, using a 512 nm laser. Spectra were collected averaging 10 scans at a resolution of 2 cm⁻¹. HRTEM images were recorded in a JEOL JEM 2100F under accelerating voltage of 200 kV. Samples were prepared by applying one drop of the suspended material in ethanol onto a carbon-coated copper TEM grid, and allowing them to dry at room temperature. XPS spectra were measured on a SPECS spectrometer equipped with a Phoibos 150 9MCD detector using a non-monochromatic X-ray source (Al and Mg) operating at 200 W. The samples were evacuated in the prechamber of the spectrometer at 1·10⁻⁹ mbar. The measured intensity ratios of the components were obtained from the area of the corresponding peaks after nonlinear Shirley-type background subtraction and corrected by the transition function of the spectrometer.

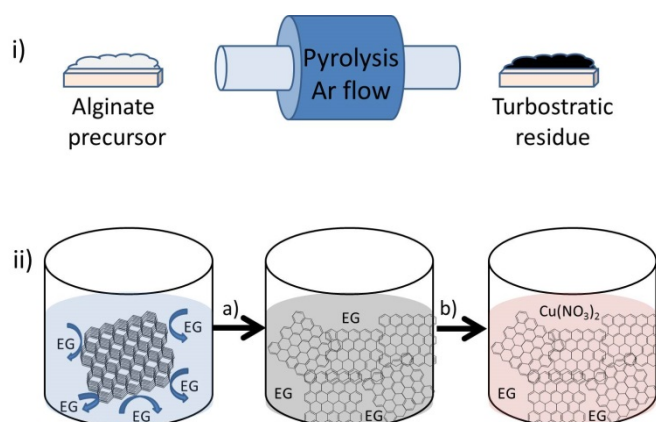
Photocatalytic measurements

A quartz photoreactor equipped with a nickel alloy thermocouple connected to a heating mantle and temperature controller was loaded with Cu₂O/G photocatalyst and placed under the light spot. H₂ and CO₂ were introduced in 4:1 molar ratio up to achieve a final pressure of 1.3 bar. Prior irradiation the photoreactor was heated at different temperatures by means of a heating mantle equipped with thermocouple and controller, and when the desired temperature was stabilized the photocatalyst was irradiated from the top (2 cm above) through a fiber optics with UV-Vis light from a 300 W Xe lamp. Note that the time required before temperature equilibration can be about 30 min. At that moment the lamp is switched on and this is the initial time of the experiments. No change in the gas phase composition was observed during the period of temperature equilibration in the dark. A picture of the experimental set up is presented in the Supplementary Information (Fig. S11, ESI). The CH₄ formation was followed by direct measurement of the reactor gases with an Agilent 490 MicroGC having two channels both with TC detectors and Ar as carrier gas. One channel has MoSieve 5A column and analyses H₂. The second channel has a Pore Plot Q column and analyses CO₂, CO and up to C₄ hydrocarbons. No evidence of the formation of CH₃OH (detectable in the MicroGC equipment) was obtained. Quantification of the percentage of each gas was based on prior calibration of the system injecting mixtures with known percentage of gases.

Results and discussion

Cu₂O/G characterization

Cu₂O/G photocatalyst has been prepared as illustrated in Scheme 1. In brief, Cu(NO₃)₂ was reduced through the polyol



Scheme 1. Cu₂O/G photocatalyst preparation. i) Pyrolysis of the alginate precursor and ii) dispersion of the turbostratic residue in ethylene glycol (EG) upon 700 W sonication for 1 h (a) and subsequent Cu(NO₃)₂ addition (b) and reduction at 120 °C for 24 h.

method²⁴ in the presence of G sheets obtained from the pyrolysis of alginate at 900 °C under Ar atmosphere and subsequent exfoliation of the carbon residue.²³ The obtained Cu₂O/G composite contained a nominal Cu content of 1.5 wt%, as confirmed by ICP-OES elemental analysis.

The defective nature of G in the Cu₂O/G samples was confirmed by Raman spectroscopy in good agreement with the reported properties of G obtained from alginate pyrolysis²³. Fig. 1 (inset) shows the corresponding D (1350 cm⁻¹), G (1580 cm⁻¹) and 2D (2700 cm⁻¹) bands expected for these defective graphene sheets. Those defects consist mainly in carbon vacancies and the presence of residual oxygen (8 wt%) remaining from the initial alginate precursor as reported before.²⁵ In addition, XRD pattern (Fig. 1) of the Cu₂O/G samples showed the typical diffraction peaks corresponding to cubic Cu₂O, and the broad diffraction peak at 2 θ about 24° corresponds to the expected diffraction for few layer G.

The presence of the Cu₂O NPs on the G sheets was confirmed by HRTEM (Fig. 2) that allowed also determination of their particle size distribution. HRTEM images show that the Cu₂O

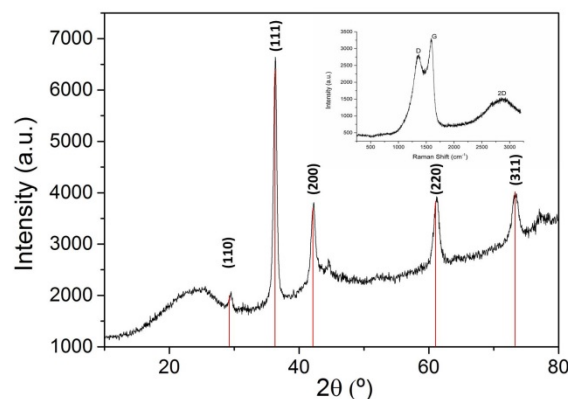


Fig. 1 XRD pattern of the Cu₂O/G photocatalyst. The peaks corresponding to Cu₂O have been indicated in red. Inset shows the Raman spectrum of Cu₂O/G recorded upon 512 nm laser excitation.

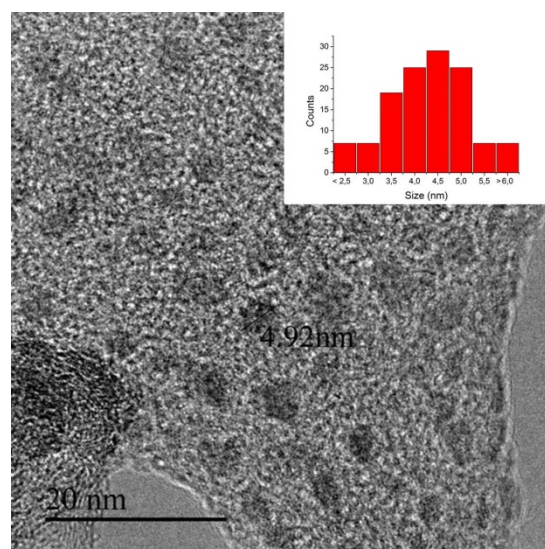


Fig. 2 HRTEM image of Cu₂O/G, in the centre of the image the size of a representative Cu₂O NP is indicated. The inset shows the size distribution histogram. Scale bar is 20 nm.

NPs were homogeneously distributed on the G sheets and its average particle size is 4.4 ± 0.86 nm, determined after measuring a statistically relevant number of MNPs.

Figure 3 shows the high resolution XPS spectrum of Cu2p 3/2 peaks and the best deconvolution to individual components. As can be observed in this figure, XPS spectrum shows the presence of Cu (I) (932.4 eV) and Cu(II) (934.4 eV) in the Cu2p 3/2 peak. The observation of a weak satellite at 943.5 eV confirmed that Cu(I) is the main component (79%), and Cu(II) was present in a lower extent (21%). Auger peak indicates that the presence of metallic Cu in the outermost layers of the Cu₂O/G sample can be ruled out (Supplementary Information Fig. S12). Since Cu(II) was not detected in XRD, it can be concluded that the presence of this oxidation state has to be limited just to a shallow outermost layer of the Cu₂O NPs.

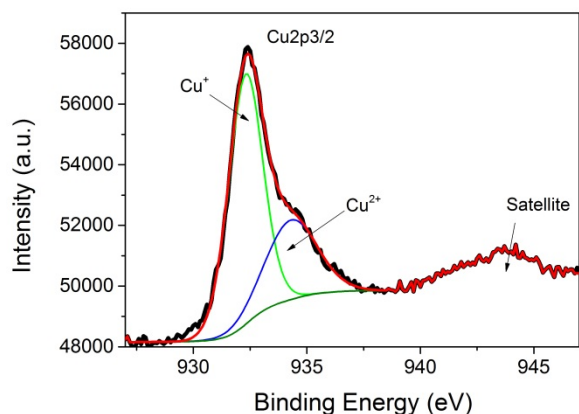


Fig. 3 High resolution XPS peak for Cu2p recorded for Cu₂O/G sample showing also its best deconvolution to individual components.

2. Photocatalytic activity

Photocatalytic CO₂ reduction tests were performed by placing the Cu₂O/G sample in a quartz photoreactor that was loaded with CO₂ and H₂ in a 1:4 stoichiometric ratio according to the requirements of eqn. 1 at a total pressure of 1.3 bar. The photoreactor was then heated at different temperatures in the range from 150 to 250 °C, and irradiation started only after temperature stabilization. The temporal evolution of CH₄ using Cu₂O/G as photocatalyst at different temperatures is presented in Fig. 4. At any of the studied temperatures the CH₄ production rate increased linearly the first 4 h (Fig. 4 inset). After that, the CH₄ production rate gradually decreased, and after 24 h 2.84% CO₂ conversion and 99% of selectivity to CH₄ were achieved at 250 °C, being as well detected CO and CH₃CH₃ at trace levels. The H₂ and CO₂ evolution over time is shown in Fig S15 in ESI.

The CH₄ production rate under illumination at different temperatures is listed in Table S11. For comparison, the photocatalytic activity of G in the absence of Cu₂O and that of commercial Cu₂O NPs (c-Cu₂O) stabilized in ethanol (< 350 nm) as well as home-made Cu₂O NPs (hm-Cu₂O) (20 nm approximately, HRTEM and XRD shown in Fig. S13 in ESI) prepared following the same ethylene glycol reduction procedure than that followed for the formation of Cu₂O/G were also determined under identical reaction conditions. It should be noted that the smaller particle size of Cu₂O when G is present in ethylene glycol should be probably due to adsorption of these NPs on the G surface that disfavors particle growth. The corresponding CH₄ production rates also included in Table S11. Blank experiments in the presence of Cu₂O/G under illumination performed at room temperature showed no detectable amounts of CH₄. Similarly, heating the photoreactor at 250 °C in the dark (lamp on, aluminum foil covering the photoreactor) led to the detection of negligible CH₄, just on the limit of the instrument response (0.005 μmol) after 24 h reaction time. In contrast, the formation of CH₄ was observed

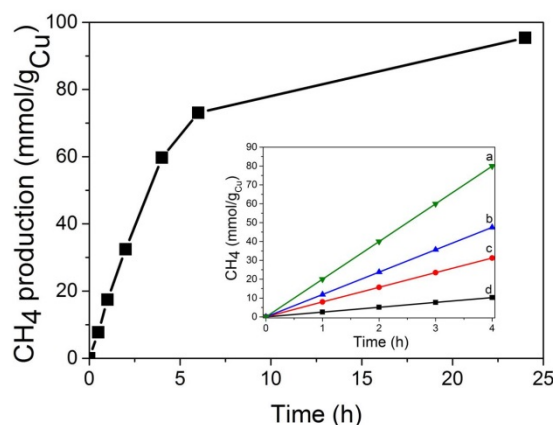


Fig. 4 CH₄ temporal profile (mmol/g_{Cu}) at 250 °C for 24 h. Inset shows CH₄ time-production (mmol/g_{Cu}) at different temperatures under illumination with a Xenon lamp of 300 W at different temperatures (a: 250 °C, b: 225 °C, c: 200 °C and d: 150 °C). Reaction conditions: Cu content 0.56 mg. P_{H₂} = 1.05 bar, P_{CO₂} = 0.25 bar.

when the photoreactor was irradiated at temperature above 150 °C in the presence of Cu₂O/G.

From Table S11 it can be concluded that G is inactive for CH₄ production under optimal operation conditions (250 °C under illumination), while c-Cu₂O and hm-Cu₂O NPs presented a CH₄ production rate of 2.69 and 0.01 mmol/g_{Cu}·h, respectively. It is worth noting that the hm-Cu₂O NPs demonstrated much lower photocatalytic activity than the commercial ones. This low photocatalytic activity of hm-Cu₂O NPs is probably due to their faster deactivation by H₂ reduction to inactive Cu NPs as it would be commented below for the case of Cu₂O/G.

When Cu₂O/G was used as photocatalyst under these reaction conditions, a CH₄ production rate of 14.93 mmol/g_{Cu}·h was obtained which, to the best of our knowledge, is the highest CH₄ production rate reported for gas-phase methanation reaction at temperatures below Sabatier reaction (<300 °C) using semiconductor-based photocatalysts²⁶⁻²⁹. Table S12 in the supplementary information provides reported data about photo-assisted methanation production rates and the corresponding relevant conditions. The maximum apparent quantum yield achieved for this reaction for Cu₂O/G at 250 °C was 7.84 % (calculated in the first 4 h of irradiation taking into account the 250-360 nm active wavelength range for the photocatalyst).

Comparison of the activity of G, c-Cu NPs or hm-Cu NPs indicates that the photoactive component appear to be Cu₂O behaving as semiconductor, in agreement with its known photocatalytic activity. However, the remarkably higher photocatalytic activity of Cu₂O/G with respect to the other Cu₂O samples evidences that G is not only acting as support of Cu₂O NPs, but also there must be a synergy between the Cu₂O NPs and G favouring the photoassisted reaction. In order to confirm this synergy a series of photocatalysts in which a constant amount of hm-Cu₂O was supported on increasing amounts of G to obtain samples with different hm-Cu₂O-to-G ratios were

prepared. The resulting composites were used as photocatalysts in the photoassisted methanation reaction and the CH₄ obtained under 200 °C and 200 mW/cm² illumination measured (Fig. S14 in ESI). As can be observed, the CH₄ production increased with the percentage of G in the composite photocatalyst, indicating that G is enhancing the CH₄ production. A reasonable proposal is that G contributes to enhance the efficiency of photo-induced charge separation, by migration of conduction band electrons on Cu₂O to G. Moreover, it should be noted the high selectivity to CH₄ production (> 99 %) obtained with the Cu₂O/G photocatalysts, although CH₃CH₃ and CO were also detectable at trace levels. Labelled ¹³C¹⁸O₂ was used in order to confirm the origin of the C source in the CH₄ production and the formation of H₂O as expected according to eqn. 1. Using ¹³C¹⁸O₂ as substrate the obtained gases were analysed after 4 h reaction under optimal conditions by GC-MS spectroscopy (see Fig. S16 in ESI), obtaining a mixture of 14% of ¹²CH₄ and 86% of ¹³CH₄, calculated from the relative intensity of the 17 vs. corrected 16 peak corresponding to ¹³CH₄ respect to unlabelled ¹²CH₄. This result indicates that most, but not all, of the produced CH₄ comes from the ¹³C¹⁸O₂ in the gas phase. The most likely origin of the unlabelled 14% ¹²CH₄ is the carbon atoms of G forming part of the Cu₂O/G photocatalyst. It could be that G undergoes partial decomposition into CO/CO₂ during reaction, contributing to the overall CH₄ formation. Please note that G used in this study comes from pyrolysis of alginate biopolymer, containing a residual 8 wt.% of oxygen in its composition. It should be noted that although under the present experimental conditions G irradiation of G does not result in CH₄ formation, as confirmed by a control experiment, the presence of Cu₂O as photocatalyst in Cu₂O/G can probably favour some G decomposition. In the same experiment using ¹³C¹⁸O₂, formation of H₂¹⁶O and H₂¹⁸O was also detected (See Fig. S16 in ESI). This observation confirms H₂O formation in the methanation as indicated by eqn. 1, based on the observation of H₂¹⁸O. The origin of H₂¹⁶O should be the residual oxygen content of G, concomitant with the formation of ¹²CH₄ and the O atoms of Cu₂O that can become reduced to Cu metal.

The influence of the temperature promoting methanation was established by carrying out the reaction at different temperatures and studying the CH₄ evolution, as evidenced in Fig. S17 in ESI. As commented earlier, the photocatalytic CO₂ reduction did not take place under illumination at room temperature. At 150 °C the production rate was only a 13 % of the amount observed at 250 °C. The CH₄ production increased exponentially with temperature, following the Arrhenius eqn. (eqn. 2) under constant light intensity of 200 mW/cm². From the influence of the temperature on the initial reaction rate, an apparent activation energy for the photo-assisted CO₂ methanation could be estimated a value of 28.8 kJ/mol.

$$K(T) = A \cdot e^{-\frac{E_a}{RT}} \quad (2)$$

The role of light promoting methanation was confirmed by studying the effect of light intensity on the photoassisted CH₄ production. Fig. S17 in ESI also shows the dependence of

methanation with light intensity. The CH₄ production was very small at 250 °C under light intensities below 100 mW/cm². From this threshold, the rate increased rapidly up to light intensity values close to 200 mW/cm². Further increase in light intensity produced a minor increase in the production rate, probably due to saturation effects in which the maximum carrier density is close to be reached.

In a previous related process, Linic et al. have observed an enhanced propylene epoxidation selectivity when CuO NPs supported on SiO₂ were illuminated at 200 °C with high light intensity (500 mW/cm²). In that case it was demonstrated light-induced change in the Cu oxidation state from +2 to +1 occurring beyond a critical light intensity threshold (500 mW/cm²).³⁰ In the present case, selectivity to CH₄ was > 99 % independently of the light intensity and reaction temperature.

3. Mechanism

We were interested in elucidate the mechanism of the photoassisted CO₂ methanation by Cu₂O. First, in order to determine whether CO₂ activation arises from photogenerated electron-hole pairs or from photothermal processes several molecules with different oxidation potentials were added as sacrificial electron donor agents to the reaction mixture (Fig. 5). A trend between the sacrificial molecule oxidation potential and the CH₄ evolution was observed. As can be observed in Fig. 5, the CH₄ production rate increased when the oxidation potential of the sacrificial electron donors decreased. The CH₄ production using dimethylaniline or anisole was higher respect to the reaction in the absence of any additive. Moreover, when high oxidation potential molecule as p-xylene was used, the CH₄ evolution was suppressed.

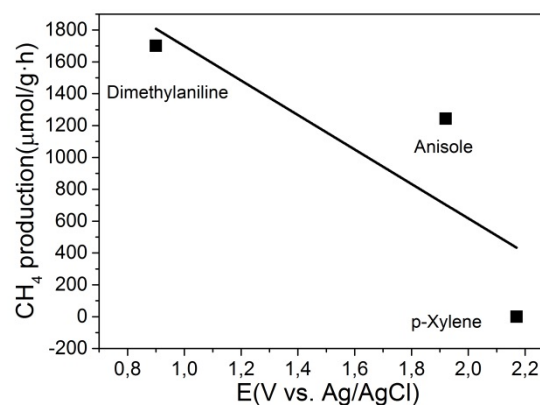


Fig. 5. CH₄ production as function of the sacrificial agent oxidation potential. The CH₄ production rate was measured under constant light intensity of 200 mW/cm² from a 300 W Xe lamp at 200 °C. Reaction time was 1h. P_{H₂} = 1.05 bar, P_{CO₂} = 0.25 bar. 20 μl of each sacrificial agent was added to the reactor vessel in each experiment.

On the other hand, a sacrificial electron acceptor (nitrobenzene) was used instead of donors, and in agreement with a photoinduced charge separation mechanism, undetectable CH₄ production was observed under identical conditions used in the sacrificial electron donor experiments. It is assumed that

nitrobenzene competes favourably with CO₂ for the capture of photogenerated electrons, stopping CO₂ reduction. Further evidence of the light-induced electron transfer from the Cu₂O/G photocatalysts to CO₂ was confirmed when 322 μmol/g·h of CH₄ were obtained from photoassisted CO₂ methanation was carried out in the absence of H₂, but using instead dimethylaniline as sacrificial electron donor. In the absence of H₂, but in the presence of dimethylaniline, positive holes would be quenched by the aromatic amine and electrons in the conduction band should reduce CO₂.

On the other hand, local temperature increase of nanoparticles under light irradiation to thermally activate H₂ and promote CO₂ methanation has been demonstrated in other systems.³¹ In the present case, a light-induced local temperature increase was considered and disregarded based on the attempts to measure the instantaneous local (at nanometric length scale) temperature increase using quantum dots (QD) as temperature indicators³². It is well established that semiconducting quantum dots can exhibit notable variations in the emission quantum yields and their emissive properties as a function of the temperature. Therefore, these QDs can be used as local thermometers. In preliminary calibration experiments thin films (< 20 nm) of commercial core-shell CdSe@ZnS were deposited by spin coating on quartz substrates and their emission lifetime measured at different temperatures (see Fig. S18 in ESI). The emission lifetime varied from 33.9 ns at room temperature up to 5.4 ns at 150 °C. Further increase in temperature resulted in QD degradation and/or emission disappearance. Therefore, it seems that QDs can probe locally temperatures in the range from ambient to 150 °C. QD thin layers were subsequently deposited on top of Cu₂O/G thin films prepared by spin coating aqueous solutions of alginate sodium salt and Cu(NO₃)₂ on quartz substrates and pyrolyzed at 900 °C under Ar flow, as reported before³³, and QD emission lifetime measured while irradiated with the 300 W Xe lamp source used in photocatalytic experiments. If the light source would have produced local heating of the Cu₂O nanoparticles, the emission lifetime of the QD in contact with them should decrease or even disappear. Note that in these experiments the Cu₂O/G film was not heated and the purpose was to gain information about possible local temperature increase due to irradiation of Cu₂O/G at room temperature. As can be observed in Fig S16, irradiation or not with the 300 W Xe lamp to the Cu₂O/G film containing CdSe@ZnS QDs as temperature sensors did not alter the QD emission lifetime, failing to observe relevant variations in the lifetime values that were constant around 33 ns. The results indicate that local increase of the temperature due to light irradiation is not taking place or it cannot be detectable for CdSe@ZnS QDs.

Therefore, the correlation between the oxidation potential of electron donors and acceptor with the CH₄ production rate combined with the failure to observe light-induced local temperature increase led us to propose that the most likely mechanism for the photoassisted methanation by Cu₂O/G is the photogeneration electron-hole pairs.

These electron-hole pairs must be generated in a semiconductor upon light excitation. Cu₂O is a semiconductor known to exhibit light absorption in the UV-Vis region with 1.94 eV band gap³⁴. However, in the present Cu₂O/G system when a UV cut-off filter (>360 nm) was used formation of CH₄ was not observed, both in c-Cu₂O NPs as Cu₂O/G samples (Table S11). On

the contrary, methanation could be successfully performed using Cu₂O/G as photocatalyst by irradiating with quasi monochromatic 254 nm light. As can be observed in Table S11, the irradiation at 250 °C of Cu₂O/G with 254 nm monochromatic light produced a CH₄ production rate of 810 μmol/g_{Cu}·h. Therefore, it can be concluded that the photocatalytic activity of Cu₂O/G for methanation reaction comes from the high energy absorbed photons in the UV region (<360 nm).

To understand this wavelength dependence, the diffuse reflectance spectra of G and Cu₂O/G were recorded (Fig. S19a in ESI). As it can be observed there, none of the two samples presents intense absorption bands in the visible region. This could be due to the small Cu₂O content on G (1.5 wt.%), whose contribution is overlapped and masked by the most intense absorption of G (98.5 % in weight). UV-Vis spectrum of a solution of c-Cu₂O NPs in ethanol at the same concentration that exists in the Cu₂O/G samples confirms this negligible visible light absorption (see Fig. S19b in ESI). However, Cu₂O exhibits a much more intense absorption band in the UV region, below 360 nm and it seems that it is this strong absorption band that upon excitation is the one that is being responsible for methanation.

Two main reaction pathways have been proposed in the complete CO₂ methanation. Scheme S11 in ESI summarizes the proposed reaction pathways. According to these routes, the CO₂ methanation can be carried out through initial hydrogen incorporation (associative) or by detachment of oxygen atoms (dissociative)³⁵. In order to distinguish between these two possible routes, CO instead of CO₂ and H₂ was introduced into the photoreactor as substrate under methanation conditions. The CH₄ production rate using CO as reactant was approximately 2-fold faster than using CO₂ (see Fig. S110 in ESI), indicating that in the present case dissociative mechanism could take place easily and that in this route the first elementary reaction (from CO₂ to CO) would be rate determining step, occurring slower than the following paths. This would explain why CO is not present in significant concentrations, due to its much faster conversion compared to CO₂ under the reaction conditions.

Although the next dissociative step from CO to C is difficult to be evaluated due to the photocatalyst composition based on carbon, an additional experiment was performed to provide some evidence of the occurrence of the last step of the dissociative path involving the intermediacy of methylene (:CH₂) reacting with H₂. For this purpose, a small amount of CH₄ was added to the initial reactants in order to monitor the CH₃CH₃ production. It is known that :CH₂ can insert into C-H bonds, being responsible for the chain growth in processes like Fisher-Tropsch. Therefore, the increase of CH₃CH₃ production would be an indirect proof of the generation of :CH₂ intermediate and subsequent insertion into the C-H bond of the introduced CH₄ molecules, providing support to the dissociative reaction pathway. Furthermore, ¹³C-labelled CH₄ was also used in this experiment and the GC-MS analysis confirmed that the CH₃CH₃ formed in the reaction derives from the reaction of labelled ¹³CH₄ with ¹²CO₂ by monitoring ¹³CH₃-¹²CH₃.

Unfortunately, the possibility of the occurrence also of associative pathways using formaldehyde or formic acid as

starting reactants could not be addressed due to the instability and spontaneous decomposition of these two compounds at the reaction conditions (200 °C). Despite this, the fast CO methanation and the formation of the :CH₂ intermediate together with the instability of formaldehyde under the reaction conditions point out to the dissociative CO₂ methanation as the most probable mechanistic route.

As commented in detail earlier, the temperature has a major role in this photocatalytic CO₂ methanation. In order to gain insights into the role of the temperature, several control reactions were carried out introducing increasing amounts of H₂O in the reaction media at initial reaction times and the methanation carried out at different temperatures.

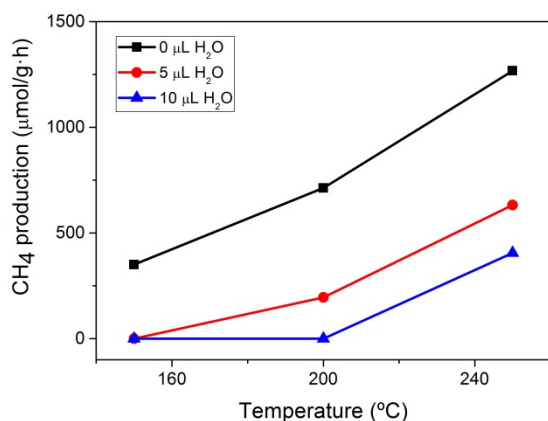


Fig. 6 CH₄ production rate in function of temperature upon addition of H₂O aliquots. The CH₄ production rate was measured under constant light intensity of 200 mW/cm² from a 300 W Xenon lamp. Reaction time was 1h. P_{H₂} = 1.05 bar, P_{CO₂} = 0.25 bar.

The hypothesis is that the temperature is needed to desorb H₂O formed as product in the methanation reaction (see eqn. 1). Thus, Fig. 6 shows the initial CH₄ production rate upon H₂O addition in the reaction at different temperatures. As can be observed the presence of small amounts of H₂O decreases the CH₄ evolution at all temperatures depending on the amount of H₂O added. Note that the maximum amount of H₂O added on the experiments of Fig. 6 (10 μl) is much lower than the theoretical amount of H₂O formed on the methanation reaction that is estimated in 1.4 mL. These experiments indicate that H₂O formed during the reaction should inhibit the methanation reaction probably by strong adsorption on Cu₂O/G photocatalysts. If this is the case, an increase in temperature should favor H₂O desorption, and therefore, enhance CH₄ evolution.

4. Photocatalyst stability

The stability of Cu₂O/G in the methanation reaction was investigated by performing prolonged 48 h experiment, and the result is presented in Fig. 7.

In this long irradiation experiment, CH₄ evolution was observed only the first 6 h, remaining practically constant the CH₄ concentration after this period, in spite that a considerable

percentage of CO₂ and H₂ was still present. This indicates complete photocatalyst deactivation.

In order to determine the origin of the Cu₂O/G deactivation, the sample was washed with base (triethanolamine aqueous solution at pH 9), but HPLC analysis of the washings did not allow detection of any by-product that could be adsorbed on the Cu₂O/G catalyst acting as poison. Particularly it rules out formic acid or oxalic acids as adsorbed products. Moreover, HRTEM images of deactivated Cu₂O/G photocatalysts after reaction were also acquired, but no differences in the material morphology or size distribution with respect to these of the fresh Cu₂O/G sample were found (see Fig. S111 in ESI). Finally, XRD pattern of the deactivated Cu₂O/G photocatalysts after reaction was compared with the diffraction peaks of the fresh photocatalysts prior to the reaction and they are shown in Fig. 7 inset.

As can be observed in Fig. 7 inset, the diffraction peaks of fresh Cu₂O/G corresponding to Cu (I) oxide have evolved to those corresponding to Cu metal. This result is indicating that under the reaction conditions at 250 °C in H₂ atmosphere, the Cu₂O becomes reduced to Cu⁰. To confirm that this reduction from Cu^I to Cu⁰ is due to the presence of H₂ and the reaction temperature and not to the action of the photocatalytic reaction, Cu₂O/G sample was submitted at 250 °C in H₂ atmosphere in dark conditions, and XRD pattern confirmed the complete Cu (I) oxide reduction to Cu⁰. Interestingly, in an alternative control experiment, light-assisted CO₂ methanation was attempted under optimal conditions using the reduced Cu/G formed by H₂ treatment of Cu₂O/G. No formation of detectable CH₄ amounts was observed, indicating that Cu⁰ is not active for this reaction under these conditions.

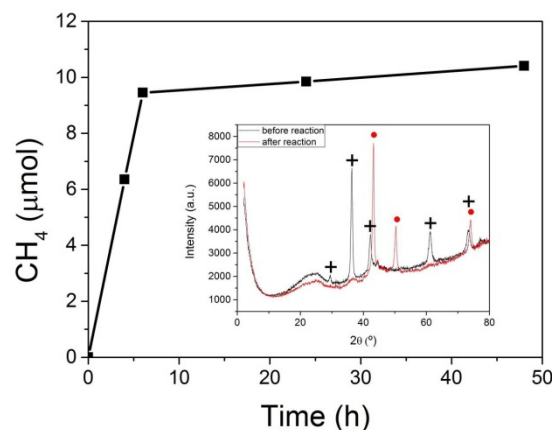


Fig. 7 Time-CH₄ evolution plot in a 48 h photoassisted methanation using Cu₂O/G photocatalyst. The inset shows the XRD pattern of just prepared Cu₂O/G photocatalyst (black crosses) and after submitting it 4 h under the photoassisted reaction conditions (red dots). Reaction conditions: Cu content 0.56 mg. P_{H₂} = 1.05 bar, P_{CO₂} = 0.25 bar, temperature 250 °C, irradiation power density 200 mW/cm² from a 300 W Xe lamp.

Therefore, it can be assumed that the active Cu₂O supported in G becomes reduced to Cu⁰ during the course of the photocatalytic reaction and this transformation is the origin of the long-term catalyst instability. Notice that this deactivation mechanism is a consequence of the temperature of the system

and the presence of H₂ and not really due to the photocatalytic mechanism.

To overcome this limitation, deactivated Cu₂O/G catalyst was submitted to reactivation by heating the photocatalyst at 250 °C in air for 4 h, testing the activity of the reoxidized material in subsequent reuses. Although partial reoxidation of the photocatalysts was accomplished (see Fig. S112a in ESI), second and third re-uses showed that the reactivated Cu₂O/G photocatalyst by thermal annealing by oxygen exhibits only a part of the initial CH₄ production obtained with the fresh Cu₂O/G material (Fig. S112b in ESI). This partial reactivation is probably due to the inefficient re-oxidation process which is able to re-oxidize to Cu₂O only the outermost part of the Cu nanoparticles, resulting, therefore, in a lower photocatalytic activity than the fresh material.

To increase the stability of Cu₂O/G under the reaction conditions, an alternative approach consisting in coating Cu (I) by a thin layer of Au was explored. In this approach, Cu₂O/G photocatalyst was impregnated with diluted solutions of HAuCl₄ (0.15 – 0.35 wt.%) and used in the photoassisted methanation reaction without further treatment. Under the reaction conditions, Au (III) should become immediately reduced to Au (0), coating Cu₂O NPs with a Au layer thin enough to still allow charges to reach CO₂ and H₂, performing the methanation reaction. Au was selected for this purpose due to its noble character and conductive properties.

Fig. 8 shows the photoassisted CO₂ methanation at optimal conditions using Cu₂O/G photocatalyst containing different amounts of Au. As can be observed, a 3-fold decrease in the CH₄ production rate was obtained when 0.15 wt.% Au was deposited compared with the sample without Au. However, the 0.15 wt.% Au-Cu₂O/G sample exhibited extended stability until 72 h while the uncoated Cu₂O/G sample presented complete deactivation in 48 h. Further increase in the Au loading (0.25 wt.% Au) resulted in improved activity and stability, although higher concentration (0.35 wt.% Au) resulted detrimental for the CH₄ formation under the same conditions. We cannot discard the presence of individual Au NPs in the G substrate. For that reason, we performed a blank experiment using a photocatalysts containing exclusively Au NPs supported on G prepared following the same procedure as the Au coating. However, undetectable amounts of CH₄ were found under optimal reaction conditions with this Au/G photocatalyst.

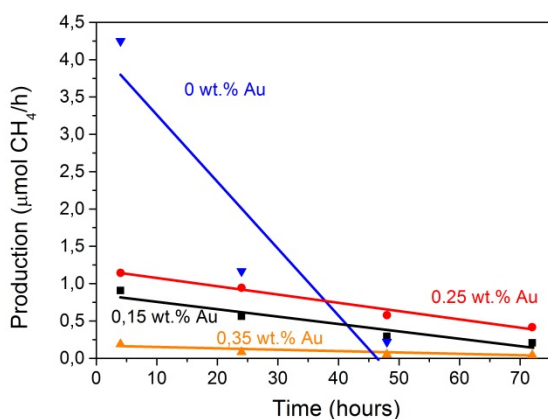


Fig. 8 CH₄ production rate using 0, 0.15, 0.25 and 0.35 wt.% Au loading in the Cu₂O/G photocatalyst. The CH₄ production rate

was measured under constant light intensity of 200 mW/cm² from a 300 W Xe lamp. P_{H₂} = 1.05 bar, P_{CO₂} = 0.25 bar.

Although further studies are need to clarify the influence of the presence of Au on the stability of Cu₂O/G as photocatalyst, the data obtained show that coating Cu₂O by Au decreases CH₄ production rate, but increases its stability. Under optimal Au percentages, CH₄ production rates are still about 50 % of the initial value for the fresh Au-Cu₂O/G material, while the pristine Cu₂O/G photocatalyst undergoes complete deactivation in less than 48 h. These findings open further research to improve NP coating and to investigate different coatings in order to extend the stability of unstable photocatalysts, while preserving much of their photocatalytic activity.

Conclusions

The present manuscript describes the photocatalytic activity of Cu₂O nanoparticles supported on G in the photoassisted gas-phase, CO₂ methanation reaction reaching a specific CH₄ production rate of 14.93 mmol/g_{Cu₂O}·h and apparent quantum yield of 7.84 % when the reaction is carried out at 250 °C under 200 mW/cm² power irradiation. Experimental evidence points out that the most probable reaction mechanism occurs through light-induced generation of electron-hole pairs, while no evidence for a local increase of temperature induced by light has been obtained. Nevertheless, the reaction temperature has been found to play a key role, by favouring H₂O desorption formed during the reaction from the Cu₂O/G photocatalyst. Moreover, catalytic data support the dissociative CO₂ methanation as the most probable mechanistic route. Finally, it has been observed that Cu₂O nanoparticles become reduced to Cu metal during reaction, limiting the long-term stability of this photocatalyst. The possibility to reoxidize the Cu₂O/G photocatalyst to recover their activity or to coat Cu₂O NPs with a thin Au overlayer to increase their stability have been explored.

Acknowledgements

Financial support by the Spanish Ministry of Economy and Competitiveness (Severo Ochoa, grasas, and CTQ2015-69563-CO2-R1) and by the Generalitat Valenciana (Prometeo 2013-014) is gratefully acknowledged. J. A. thanks the Universitat Politècnica de València for a postdoctoral scholarship. D. M. also thanks Spanish Ministry of Science for PhD Scholarship.

Notes and references

1. L. Yuan and Y.-J. Xu, *Applied Surface Science*, 2015, **342**, 154-167.
2. I. Ganesh, *Renewable and Sustainable Energy Reviews*, 2015, **44**, 904-932.
3. W. Tu, Y. Zhou and Z. Zou, *Advanced Materials*, 2014, **26**, 4607-4626.

4. A. Corma and H. Garcia, *Journal of Catalysis*, 2013, **308**, 168-175.
5. Y. Izumi, in *Advances in CO₂ Capture, Sequestration, and Conversion*, American Chemical Society, 2015, vol. 1194, ch. 1, pp. 1-46.
6. T. Inoue, A. Fujishima, S. Konishi and K. Honda, *Nature*, 1979, **277**, 637-638.
7. J. Albero and H. García, in *Heterogeneous Photocatalysis: From Fundamentals to Green Applications*, eds. J. C. Colmenares and Y.-J. Xu, Springer-Verlag Berlin Heidelberg, 1 edn., 2016, DOI: 10.1007/978-3-662-48719-8, ch. 1, p. VIII 416.
8. O. Ozcan, F. Yukruk, E. U. Akkaya and D. Uner, *Topics in Catalysis*, **44**, 523-528.
9. F. Gonell, A. V. Puga, B. Julián-López, H. García and A. Corma, *Applied Catalysis B: Environmental*, 2016, **180**, 263-270.
10. Ş. Neaţu, J. A. Maciá-Agulló, P. Concepción and H. Garcia, *Journal of the American Chemical Society*, 2014, **136**, 15969-15976.
11. X. Xie, K. Kretschmer and G. Wang, *Nanoscale*, 2015, **7**, 13278-13292.
12. C. Lavorato, A. Primo, R. Molinari and H. Garcia, *Chemistry – A European Journal*, 2014, **20**, 187-194.
13. P. Kumar, H. P. Mungse, O. P. Khatri and S. L. Jain, *RSC Advances*, 2015, **5**, 54929-54935.
14. M. Latorre-Sánchez, I. Esteve-Adell, A. Primo and H. García, *Carbon*, 2015, **81**, 587-596.
15. X. An, K. Li and J. Tang, *ChemSusChem*, 2014, **7**, 1086-1093.
16. Z. Xiong, Y. Luo, Y. Zhao, J. Zhang, C. Zheng and J. C. S. Wu, *Physical Chemistry Chemical Physics*, 2016, DOI: 10.1039/C5CP07854G.
17. Q. Xiang, B. Cheng and J. Yu, *Angewandte Chemie International Edition*, 2015, **54**, 11350-11366.
18. F. Li, L. Zhang, J. Tong, Y. Liu, S. Xu, Y. Cao and S. Cao, *Nano Energy*, 2016, **27**, 320-329.
19. I. Shown, H.-C. Hsu, Y.-C. Chang, C.-H. Lin, P. K. Roy, A. Ganguly, C.-H. Wang, J.-K. Chang, C.-I. Wu, L.-C. Chen and K.-H. Chen, *Nano Letters*, 2014, **14**, 6097-6103.
20. Y. Lum, Y. Kwon, P. Lobaccaro, L. Chen, E. L. Clark, A. T. Bell and J. W. Ager, *ACS Catalysis*, 2016, **6**, 202-209.
21. J.-P. Zou, D.-D. Wu, J. Luo, Q.-J. Xing, X.-B. Luo, W.-H. Dong, S.-L. Luo, H.-M. Du and S. L. Suib, *ACS Catalysis*, 2016, **6**, 6861-6867.
22. W.-J. Ong, L.-L. Tan, S.-P. Chai, S.-T. Yong and A. R. Mohamed, *Nano Energy*, 2015, **13**, 757-770.
23. C. Lavorato, A. Primo, R. Molinari and H. García, *ACS Catalysis*, 2014, **4**, 497-504.
24. A. Primo, I. Esteve-Adell, J. F. Blandez, A. Dhakshinamoorthy, M. Alvaro, N. Candu, S. M. Coman, V. I. Parvulescu and H. Garcia, *Nat Commun*, 2015, **6**.
25. M.-M. Trandafir, M. Florea, F. Neaţu, A. Primo, V. I. Parvulescu and H. García, *ChemSusChem*, 2016, **9**, 1565-1569.
26. K. Li, B. Peng and T. Peng, *ACS Catalysis*, 2016, **6**, 7485-7527.
27. J. L. White, M. F. Baruch, J. E. Pander, Y. Hu, I. C. Fortmeyer, J. E. Park, T. Zhang, K. Liao, J. Gu, Y. Yan, T. W. Shaw, E. Abelev and A. B. Bocarsly, *Chemical Reviews*, 2015, **115**, 12888-12935.
28. A. V. Puga, *Topics in Catalysis*, 2016, **59**, 1268-1278.
29. Y. Izumi, *Coordination Chemistry Reviews*, 2013, **257**, 171-186.
30. A. Marimuthu, J. Zhang and S. Linic, *Science*, 2013, **339**, 1590-1593.
31. J. Ren, S. Ouyang, H. Xu, X. Meng, T. Wang, D. Wang and J. Ye, *Advanced Energy Materials*, 2017, **7**, n/a-n/a.
32. L. Liu, K. Zhong, L. Meng, D. V. Hemelrijck, L. Wang and C. Glorieux, *Journal of Applied Physics*, 2016, **119**, 224902.
33. D. Mateo, I. Esteve-Adell, J. Albero, A. Primo and H. García, *Applied Catalysis B: Environmental*, 2017, **201**, 582-590.
34. X. Liu, Z. Li, W. Zhao, C. Zhao, Y. Wang and Z. Lin, *Journal of Materials Chemistry A*, 2015, **3**, 19148-19154.
35. B. Miao, S. S. K. Ma, X. Wang, H. Su and S. H. Chan, *Catalysis Science & Technology*, 2016, **6**, 4048-4058.